A Seasonal Precipitation and Stream Flow Hindcast and Prediction Study in the Western United States during the 1997/98 Winter Season Using a Dynamic Downscaling System

JINWON KIM AND NORMAN L. MILLER

University of California, Lawrence Berkeley National Laboratory, Berkeley, California

JOHN D. FARRARA

Department of Atmospheric Sciences, University of California, Los Angeles, Los Angeles, California

SONG-YOU HONG

Environmental Modeling Center, National Centers for Environmental Prediction, Camp Springs, Maryland

(Manuscript received 24 August 1999, in final form 8 March 2000)

ABSTRACT

The authors present a seasonal hindcast and prediction of precipitation in the western United States and stream flow in a northern California coastal basin for December 1997–February 1998 (DJF) using the Regional Climate System Model (RCSM). In the seasonal hindcast simulation, in which the twice-daily National Centers for Environmental Prediction–National Center for Atmospheric Research reanalysis was used for the initial conditions and time-dependent boundary forcing, RCSM has simulated realistically the temporal and spatial variations of precipitation in California and stream flow in a northern California coastal basin. For the headwater basin of the Russian River in the northern California Coast Ranges, the Topography-Based Hydrologic Model (TOPMODEL) forced by observed daily precipitation resulted in a correlation coefficient of 0.88 between observed and simulated DJF stream flow. In the coupled stream flow hindcast, the authors obtained a correlation coefficient of 0.7 between simulated and observed stream flow for the same period. The coupled hindcast has generally overestimated (underestimated) low (high) flow events in the basin. Errors in the simulated stream flow were due mostly to the errors in the simulated precipitation. A seasonal hydroclimate prediction experiment, in which RCSM was nested within the global forecast data from the University of California, Los Angeles, GCM, has predicted well the season-total precipitation in the western United States. Temporal variations of predicted precipitation were affected strongly by the predictability of the general circulation model. The predicted DJF-total snowfall agrees well with the snowfall simulated in the hindcast, especially in the central Cascades and the Sierra Nevada, where snowfall was the heaviest.

1. Introduction

Accurate diagnostics and prediction of seasonal hydroclimate is crucial for water resources management and flood preparation in the western United States. Rainfall-driven coastal basins, characterized by steep terrain and narrow valleys, often experience localized heavy precipitation and flooding during winter seasons. Heavy snowfall in high elevations along the Cascades, the Sierra Nevada, and the Rocky Mountains is a major source of water supply during summer seasons. This extreme seasonal bias in precipitation and the steep terrain require long-term planning for water resources management and preparation for natural disaster for this region. Advanced predictions and timely diagnosis of seasonal hydroclimate such as precipitation, snow cover, and stream flow can help to improve operations of water storage facilities, which is crucial for achieving a balance between flood control and water storage along heavily controlled rivers in the region.

The complexity of the dynamical and physical processes that determine the hydroclimate of the western United States requires a reliable downscaling system. Downscaling coarse-resolution data to the scales useful for regional-scale climate predictions and climate-impact assessment has been a growing concern (e.g., Lettenmaier and Gan 1990; Mearns et al. 1992; Miller 1993; Hostetler 1994; Kim et al. 1998a). Important hydroclimate features of the western United States vary

Corresponding author address: Dr. Jinwon Kim, MS90-1116, University of California, Lawrence Berkeley National Laboratory, 1 Cyclotron Road, Berkeley, CA 94720.
E-mail: jkim@lbl.gov

as a function of terrain (Roads et al. 1994; Leung and Ghan 1995; Kim and Soong 1996; Soong and Kim 1996; Kim 1997; Kim et al. 1998a). Spatial distribution of precipitation in the western United States is closely correlated with the major mountain ranges such as the Coast Ranges, the Cascades, the Sierra Nevada, and the Rocky Mountains. A significant portion of precipitation in high elevations is snow (Cayan and Roads 1984; Kim 1997). The surface snow budget, which determines the amount of snow cover at the end of the winter season, is affected strongly by finescale variations in terrain elevation. Snow cover is one of the hydroclimate components that require close examination under climate change scenarios, because shifts in global temperatures and associated large-scale circulation may affect the amount and timing of snowfall, snowmelt, and runoff. Spatial scales of orographic variation that are important for basin-scale snow budget and hydrologic processes are much smaller than typical resolutions of general circulation models (GCMs). Hence, assessments of basin-scale hydrologic processes and climate effects on various sectors such as water resources, crop and forest production, and ecosystem response require reliable downscaling methods to obtain fine scale information.

Statistical downscaling of GCM-simulated climate data (Barnett 1995; Wilby et al. 1998) may be useful if two conditions are met: 1) there are sufficient historical data for generating probability distribution functions and 2) variables of interest have well-defined statistical patterns. Insufficient or sparse historical data will not result in a robust statistical downscaling. Statistical downscaling methods also are limited by the fact that individual variables need variable-specific statistical models. As a result, statistically downscaled variables may not be dynamically and/or physically consistent with each other. This problem can greatly increase uncertainties in downscaled information.

Dynamic downscaling using a regional climate modeling system nested within coarse-resolution large-scale data can better maintain dynamical and physical consistency among downscaled variables than can statistical downscaling. Recently, regional climate models based on limited-area models have been developed to simulate regional-scale climate details (e.g., Giorgi et al. 1994; Kim et al. 1998a; Hong and Leetmaa 1999) with some success. A primary goal of these regional climate models is to understand better the regional climate and the effects of climate variability on various sectors of human society and environment in a physically and dynamically consistent way. Rapid improvements in computing technology and understanding of the processes involved in the earth's climate system provide an optimistic future for dynamic downscaling.

Coupled mesoscale atmosphere–stream flow simulations are emerging as an important tool for water resources management and flood forecasting (Leung et al. 1996; Miller and Kim 1996; Kim et al. 1998a; Miller et al. 1999). Short-term weather, precipitation, and stream flow forecasts provide emergency response agencies with information and guidance in projecting the part of floodplains at risk of flooding. One of the first coupled quantitative precipitation and stream flow predictions was performed during the January 1995 California floods (Miller and Kim 1996). This experimental prediction using the Regional Climate System Model (RCSM) nested within the National Centers for Environmental Prediction (NCEP) forecast data successfully predicted quantitative precipitation and peak stream flows in the headwaters of the Russian River, California.

Precipitation, snow budget, and stream flow diagnoses during winter seasons are crucial for planning summertime water supply and overall assessment of water resources in the western United States (Roads et al. 1994; Kim 1997; Kim et al. 1998a). Hence, information based on a coupled modeling system can become a useful tool to help water resource managers who need runoff and stream flow forecasts for water use and reservoir control. Seasonal hydroclimate forecasts, one of the newly emerging thrust areas of the National Weather Service and the numerical forecast community, are important for long-term planning and assessment of water resource management, agriculture, ecosystems, and emergency response preparations.

In this study, we investigate the skill of RCSM in simulating precipitation in the western United States for three winter months, December 1997–February 1998 (hereinafter DJF). We present results from a seasonal climate prediction experiment that utilizes RCSM-based downscaling of the global climate forecast data generated from the NCEP sea surface temperature (SST) forecast and the University of California, Los Angeles, atmospheric GCM (UCLA AGCM) forecast. In the following section, we present brief descriptions of RCSM and its component models and a description of a hydroclimate downscaling method used in RCSM. The parameter optimization and verification of the Topography-Based Hydrologic Model (TOPMODEL; Beven and Kirkby 1979; Duan and Miller 1997), for the Hopland basin, the headwater of the Russian River basin, is discussed in section 3. Results from the RCSM-based seasonal climate hindcast and seasonal climate prediction for the 1997/98 winter are presented in sections 4 and 5, respectively.

2. Model and experiment description

The primary function of RCSM is to downscale the large-scale data from GCMs and analyses for regional climate and climate impact assessment studies using physically based models for the atmosphere, land surface, hydrologic processes, water quality, and various effects assessments. RCSM and its modeling components have been applied successfully for seasonal hydroclimate studies, short-term weather and stream flow predictions, and water resources studies for the western United States, eastern Asia, and northeastern Australia.

Below, we present a brief description of the data flow used in the seasonal-scale hindcast and prediction experiments presented in the following sections.

The core of the dynamic downscaling in RCSM is the Mesoscale Atmospheric Simulation (MAS) model. MAS is a primitive-equation, limited-area model that includes a third-order accurate advection scheme (Tackacs 1985) and a comprehensive set of parameterizations for calculating atmospheric radiative transfer, cloud microphysics, turbulent transport, and cumulus convection. Details of the MAS formulation were presented by Kim and Soong (1996) and Soong and Kim (1996). One important improvement in MAS is the inclusion of the NCEP cumulus convection scheme (Pan and Wu 1995; Hong and Pan 1998) to compute convective condensation and heating. In comparison with an earlier version of MAS that used a Kuo-type scheme, the version that uses the NCEP cumulus scheme has reduced greatly the number of excessive local precipitation events, especially during the summertime.

Heat and moisture exchanges between the atmosphere and the land surface are computed by the interactively coupled Soil–Plant–Snow (SPS) model (Kim and Ek 1995). The SPS model predicts volumetric soil moisture content, soil temperature, water-equivalent snow cover, and canopy water content. Diagnostic variables in the SPS model include surface temperature, surface mixing ratio, runoff, and drainage. Details of the SPS model formulation can be found in Mahrt and Pan (1984), Pan and Mahrt (1987), Kim and Ek (1995), and Chang et al. (1999).

Stream flow simulation for the Hopland basin was performed using a semidistributed version of TOPMODEL (Beven and Kirby 1979; Duan and Miller 1997; Kim et al. 1998a; Miller et al. 1999) that is one-way coupled to the MAS fields. This basin is the headwater of the Russian River in the northern California Coast Ranges and is characterized by steep terrain. TOPMODEL uses distribution functions to maintain information on spatial variability of hydrologic characteristics such as surface topography. Topographic distribution functions partially control surface and subsurface flow rates by assuming that the water-table depth is parallel to the terrain surface. Net precipitation sequentially fills the interception zone, then the infiltration zone, and the saturation zone. Infiltration is modeled using the Green–Ampt assumption (Green and Ampt 1911; Beven 1984). Saturation deficit is determined via the topographic index, a scaling parameter that describes a decrease in transmissivity with depth, and the antecedent saturation deficit (Beven et al. 1984). Subsurface flow is defined as a power function of the transmissivity and the ratio of the saturation deficit to the scaling parameter (Ambroise et al. 1996; Duan and Miller 1997). TOPMODEL is used widely in the research community for basin-scale stream flow and hydrologic studies (e.g., Sivapalan et al. 1990; Wood et al. 1990; Seibert et al. 1997). We have been testing TOPMODEL for coupled operational stream flow prediction (Miller and Kim 1996; Miller et al. 1999) for which the MAS-predicted forcing is used to drive TOPMODEL.

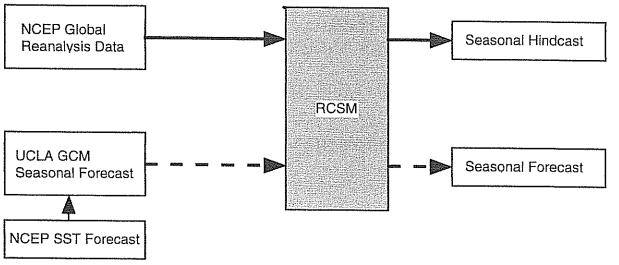

FIG. 1. A schematic illustration of the nesting of models and data flow for seasonal hindcast and seasonal forecast.

The UCLA AGCM simulates the global atmosphere from the earth's surface to the stratopause, which is set at the 1-hPa level. The model includes parameterizations of major physical processes in the atmosphere, including solar and terrestrial radiative transfer, cumulus convection, and the planetary boundary layer. Past applications of the model have shown that it can very accurately simulate major time-averaged features of the global atmospheric circulation (e.g., Suarez et al. 1983; Y. Kim et al. 1998; Li and Arakawa 1999). In addition, the performance of the model in simulating atmospheric circulation anomalies associated with idealized tropical Pacific SST anomalies has been analyzed by Mechoso et al. (1987). A more detailed description of the most recent version of the UCLA AGCM can be found in Mechoso et al. (2000) and, at the time of writing, online at http://www.atmos.ucla.edu/esm/agcmdir.

The dynamic downscaling method used in RCSM is based on a nested modeling approach in which the MAS model is one-way nested within the large-scale data from analyses and GCMs. Downscaled variables from the MAS model then are mapped over specified geographical areas to compute downscaled forcing for assessment models that cover stream flow, agriculture, water quality, and landslide thresholds. Details of the modeling components, concepts, and downscaling methods of RCSM have been presented by Miller and Kim (1997), Miller et al. (1997), and Kim et al. (1998b).

Figure 1 illustrates the data flow for the seasonal hindcast and prediction experiments in this study. The seasonal hindcast simulation, denoted by thick solid arrows, used the NCEP–NCAR (National Center for Atmospheric Research) reanalysis data at a 2.5° × 2.5° resolution and at 12-h intervals. The seasonal climate prediction experiment started from a tropical SST anomaly prediction from the NCEP coupled atmosphere–ocean GCM. The predicted SST fields then were used to force the UCLA AGCM to produce a global prediction at a 2° lat × 2.5° long resolution. RCSM used the 12-h GCM output to simulate a fine-resolution seasonal prediction for the western United States. Details of the corresponding global forecast results are presented in Farrara et al.

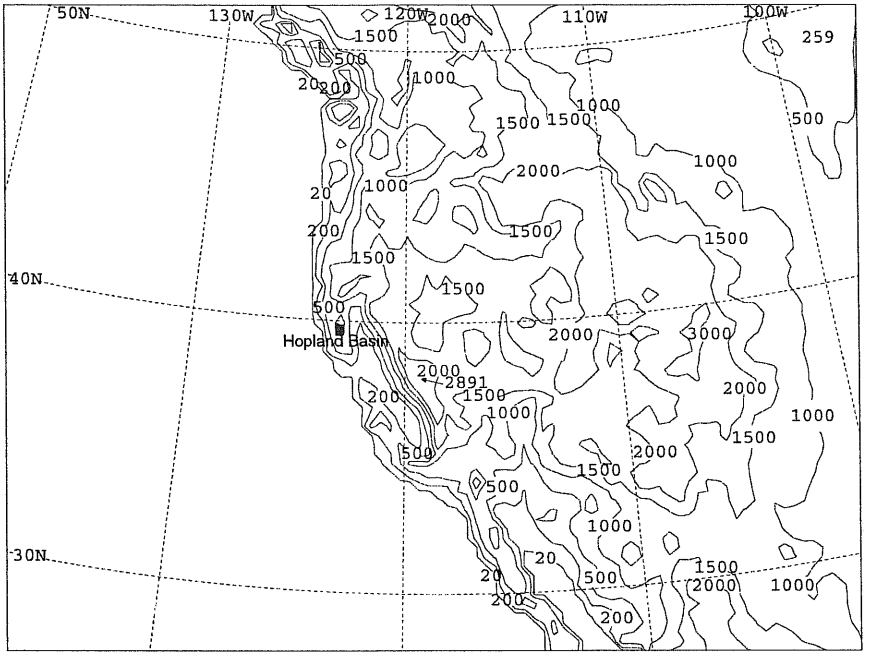

FIG. 2. Terrain elevation (m) of the western U.S. domains at a 36-km resolution.

(2000) and will not be discussed here. For the seasonal hindcast and prediction experiments in this study, RCSM was configured for a western U.S. domain with a 36 km × 36 km resolution in the horizontal and 18 irregularly spaced layers in the vertical, with the domain top at 50 hPa. The domain and terrain elevation used in this study are presented in Fig. 2.

Basin-scale hydrologic simulations using the semi-distributed TOPMODEL require area-mean input forcing data such as rainfall, air temperature, and downward radiative fluxes for each watershed. Hence, accurate calculations of the basin-average input data from the atmospheric model output are important for overall water and energy conservation in a coupled atmosphere–land surface–stream flow modeling system. To ensure this conservation in RCSM, we first map the basin boundaries computed from fine-resolution digital elevation model (DEM) data over the RCSM grids (Fig. 3). Then, area-weighted average variables are calculated as

$$P = \sum_{i,j} p_{i,j} w_{i,j} \Big/ \sum_{i,j} w_{i,j}, \tag{1}$$

where P is an average value of a variable $p_{i,j}$ over a basin, and $w_{i,j}$ is the weighting factor defined at each RCSM grid within or across the physical boundary of a basin. The summation is applied over the RCSM grids that are entirely or partially covered by a basin. The weighting factor $w_{i,j}$ is unity if a RCSM grid box (i, j) is entirely within a basin. It takes a value between 0 and 1 if only a part of the RCSM grid box covers a basin. The portion of each grid box containing the basin area is calculated from fine-resolution DEM data. This conserving area-matching procedure is important for coupled atmosphere–land surface–hydrologic simulations in the mountainous western United States, because precipitation varies rapidly as a function of terrain slope and elevation, as shown by Miller and Kim (1996) and Kim et al. (1998a). The amount of snowmelt from the SPS model was added to the MAS-simulated rainfall to compute the total liquid water input to the RCSM hydrologic models.

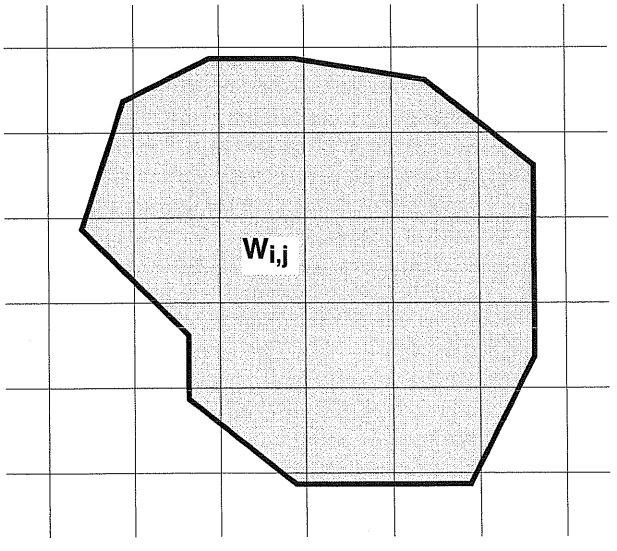

FIG. 3. A schematic illustration of calculating area-weighted basin average values from mesoscale model output.

TABLE 1. The TOPMODEL parameters for the Hopland basin.

Parameter (unit)	Description	Hopland basin
m (mm)	Scaling parameter	55.0
K [mm (day)$^{-1}$]	Saturated hydraulic conductivity	2000.0
P_{macro} (ratio)	Precipitation bypassing soil zone	0.2
Z_{tot} (m)	Total soil depth	1.2
Z_{ab} (m)	Upper soil depth	0.2
θ_{fc} (%)	Field capacity	35.0
M_λ [ln(m)]	Mean topographic index	7.18
V_λ [ln(m^2)]	Variance of topographic index	3.26
S_λ [ln(m^3)]	Skewness of topographic index	1.79
A (km^2)	Total watershed area	658.0
T_{cut} (°C)	Cutoff temperature for snowmelt	0.0
P_{imp} (ratio)	Fraction of the impervious area	0.01

3. Hydrologic model calibration

Calibration of TOPMODEL was based on sensitivity analyses to model parameters that include the scaling parameter, saturated hydraulic conductivity, field capacity, root zone depth, soil layer depths, and the mean, variance, and skewness of the topographic index. The topographic index moments were directly calculated from 3-arc-s DEM data. Soil and root depths were derived from a 12-km^2-resolution map of bedrock depth and a 3-arc-s vegetation map, respectively. Remaining parameters, that is, scaling parameter, field capacity, and saturated hydraulic conductivity, were optimized using observed data and an uncertainty optimization technique similar to Beven and Binley's (1992) generalized likelihood uncertainty estimation procedure. The optimal range of parameter values for the Hopland basin was determined via Monte Carlo simulations using observed precipitation and stream flow data for TOPMODEL. The range of individual parameter values was initialized using available basin data and information from similar basins. The range of TOPMODEL parameter values was reduced via 1000 Monte Carlo simulations in which parameter values were randomly varied within a specified range and the model efficiency (Nash and Sutcliffe 1970) was computed for each run. Values with a high efficiency were selected as a narrowed range for parameter values. An additional 1000 Monte Carlo runs were made over the reduced range for the final parameter estimation. Scatterplots (not shown) for each parameter and the corresponding model efficiency result in the calibrated parameter set.

We calibrated TOPMODEL for the Hopland basin using observed precipitation and stream flow data for a 5-yr period (1958–62) at a daily time step using the method described above. The parameter set obtained from this calibration is presented in Table 1. Because most of this basin is below the 1-km level, effects of a snow budget were not important for stream flow, eliminating additional uncertainties in model calibration. The set of optimized TOPMODEL parameter values yielded a correlation coefficient of 0.91 between the observed and simulated stream flows for the calibration period (Fig. 4a), The calibration simulation performed especially well for stream flow within the 5–15 mm day^{-1} range. Figure 4a also shows that TOPMODEL generally has underestimated (overestimated) stream flow during high flow (base flow) stage.

To examine further the optimized parameter values, we performed a verification simulation using historical forcing data for a period outside the calibration period. Figure 4b presents the observed and simulated stream flow time series for an unusually wet 2-yr verification period from fall 1982 to spring 1984 when a strong El Niño occurred. Using observed precipitation and atmospheric forcing data, TOPMODEL has simulated closely the observed stream flow. The simulated magnitude and timing of the peak stream flow agree well with observations (Fig. 4b). The TOPMODEL parameter values yielded similarly good results for other verification periods that include both wet and dry years (not shown).

4. 1997/98 winter season hindcast simulation

To evaluate the spatial distribution of the simulated precipitation, we used two analyses of the observed precipitation for the DJF period. The first precipitation analysis was produced by the National Climate Data Center (NCDC) and covers the continental United States at a 1° × 1° resolution (Fig. 5a). The second precipitation analysis, from the River Forecast Center (RFC), subjectively analyzed precipitation over California and Nevada for the same 3-month period (Fig. 5b). Note that the analysis from RFC provides much more detailed information on local precipitation than does the NCDC analysis.

In addition to precipitation analyses above, we used rain gauge and stream flow gauge data from the California Data Exchange Center/California Department of Water Resources (CDEC) for a more quantitative evaluation of the simulated precipitation and stream flow. The CDEC dataset covers only California but provides daily and monthly time series at a large number of rain gauges grouped along geographical locations and major watersheds. We used two sets of precipitation data from CDEC. Daily precipitation data were available at 88 rain gauge stations in California. The daily rain gauge data were complemented with monthly rain gauge data at 188 stations. This monthly dataset is presorted as a function of river basins. The river basins and the number of stations included in this dataset are shown in Table 2. Daily records of basin-average precipitation, stream flow at the Hopland gauge station, and reservoir discharge at the Coyote Dam also were archived to evaluate simulated basin-scale quantitative precipitation and stream flow. The natural stream flow, that is, unaffected by reservoir operation, at the Hopland stream gauge station was calculated by subtracting the amount of reservoir discharge from the stream gauge data.

The seasonal hindcast simulation covered the 3-month period of December 1997–February 1998, cap-

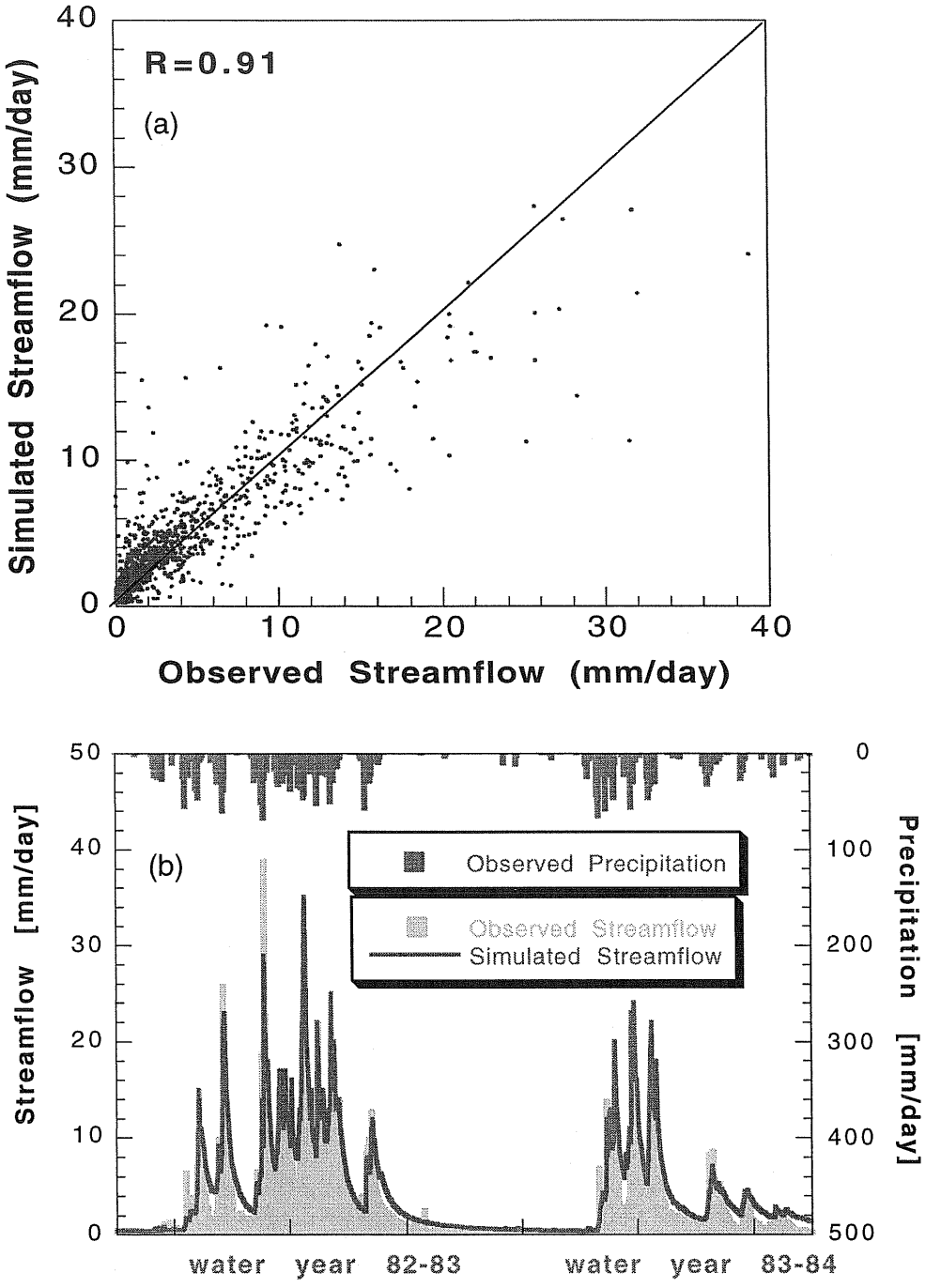

FIG. 4. (a) Observed and simulated stream flow at the Hopland basin for the 5-yr (1958–62) TOPMODEL optimization period, and (b) observed and simulated stream flow at the same basin during the verification period (1982–84). The inverted dark bar in Fig. 4b denotes the observed basin-averaged precipitation.

turing the wettest months of the season. Figure 6 illustrates the simulated monthly mean precipitation [mm (30 days)$^{-1}$] in the western United States. Simulated seasonal precipitation agrees well with the two precipitation analyses (Figs. 5a,b). MAS has simulated accurately the locations of the heaviest precipitation over the northern California Coast Ranges and along the Sierra Nevada. Within the Central Valley between the Coast Ranges and the Sierra Nevada, the simulated precipitation decreases from the north to the south as clearly seen in a more detailed RFC analysis (Fig. 5b). Precipitation decreased rapidly toward the east from the Cascades (Washington and Oregon) and the Sierra Nevada (California). This simulated spatial distribution of pre-

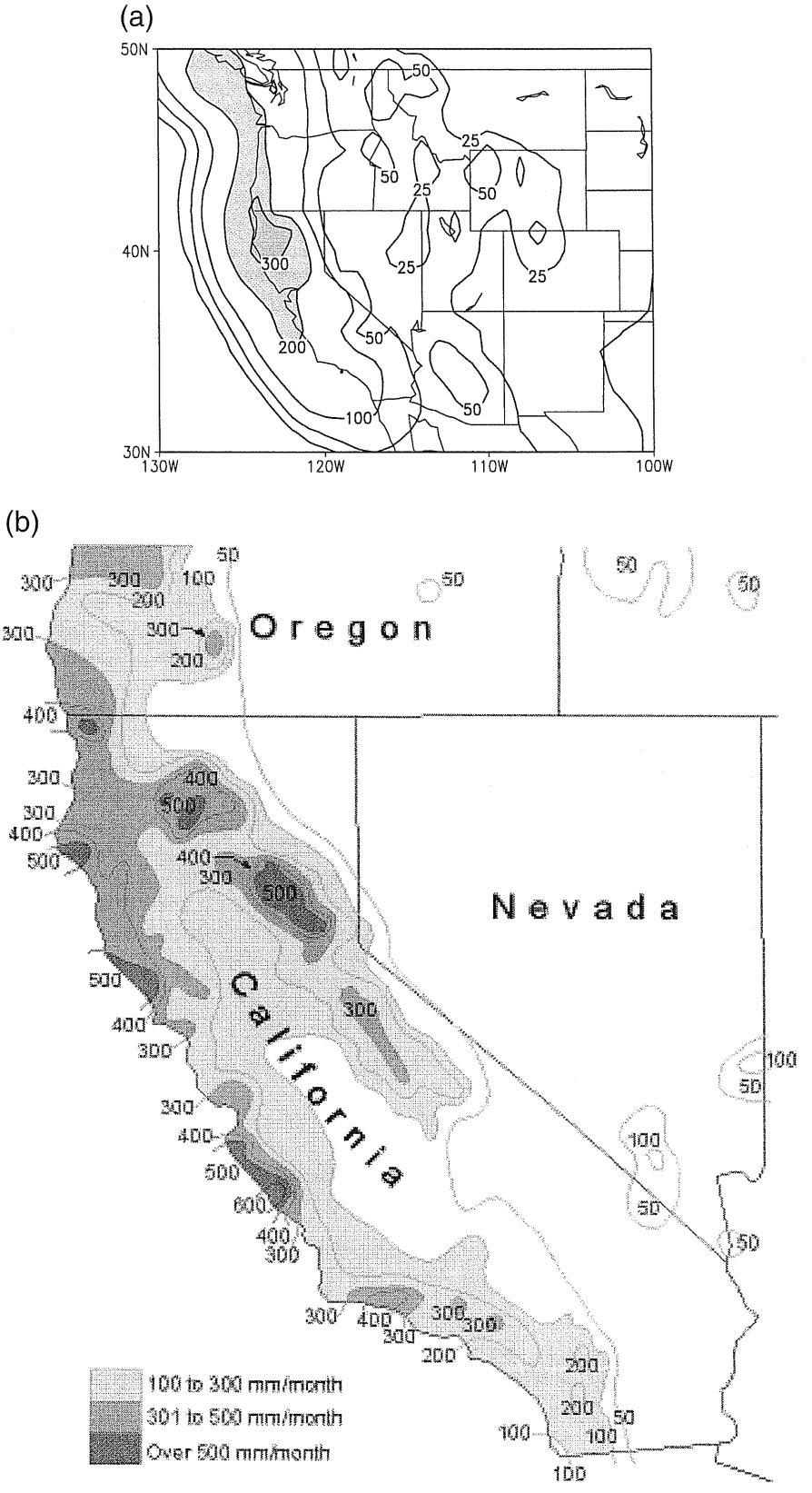

FIG. 5. Precipitation analysis (mm month^{-1}) for the 3-month period of Dec 1997–Feb 1998: (a) An NCDC analysis over the western United States at a 1° × 1° resolution, and (b) a subjective analysis over the southwestern United States from the River Forecast Center.

TABLE 2. River basins included in each subregion of California.

Subregions	River basins included	No. of rain gauge stations
Northern California coast (NCC)	Smith River, Klamath River, Trinity River, Eel River, Russian River, Coast marine, Napa River, San Francisco Bay	30
Central California coast (CCC)	San Lorenzo River, Pajaro River, Salinas River, Santa Ynez River	12
Southern California coast (SCC)	Santa Barbara coastal, Ventura–Los Angeles coastal, Santa Clara River, Los Angeles River, Santa Ana River, San Diego River	20
Northern Central Valley (NCV)	Sacramento River, Pit River, northeast Sacto Valley, western Sacto Valley, Butte Creek	27
Northern Sierra Nevada (NSN)	Feather River, Yuba River, Cache River, Mokelumne, Calaveras River, Stanislaus River, Tuolumne River	52
Southern Sierra Nevada (SSN)	Merced River, San Joaquin River, San Joaquin floor, Kinds River, Kaweah River, Tule River, Kern River, Tule Lake	47

cipitation is similar to the observed and simulated climatic data and shows that wintertime precipitation in the western United States is affected strongly by orography (Chen et al. 1995; Leung and Ghan 1995; Kim and Soong 1996; Soong and Kim 1996; Kim 1997; Kim et al. 1998a). Figures 5 and 6 also show that this simulation generally has underestimated precipitation over the Pacific west coast, especially along the coast of Washington and Oregon and the southern part of California. Along the central and southern California coast, analyzed precipitation generally exceeds 100 mm month^{-1} with local maxima over 400 mm month^{-1}, and the simulated precipitation in this region ranges from 50 to 150 mm month^{-1} with local maxima between 300 and 400 mm month^{-1}. A similar underestimation occurred along the coast of Washington and Oregon. Because orographic forcing is one of the most important factors in determining precipitation in the western United States, spatial resolution and associated terrain representation can cause a systematic bias in simulated precipitation, especially along the Pacific coast, as suggested in earlier studies. Soong and Kim (1996) and Kim et al. (1997) showed that, even at a 20-km resolution, which is a relatively high spatial resolution for regional climate simulations, the effects of terrain along the central and southern California coast were not simulated well. A typical bias from inadequate resolution of the Coast Ranges in their studies is an underestimation (overestimation) of precipitation in the central/southern California Coast Ranges (southern Sierra Nevada). Kim et al. (1997) showed that using envelope terrain along the California coast, which is equivalent to increasing terrain elevation along the Coast Ranges, largely could correct such a systematic bias in the simulated precipitation distribution. As the characteristic width of the central and southern California Coast Ranges is 10–20 km, it may require a spatial resolution of at least 10 km to represent properly the effects of coastal terrain in this region.

The RCSM-simulated precipitation is evaluated further using the available rain gauge data within California

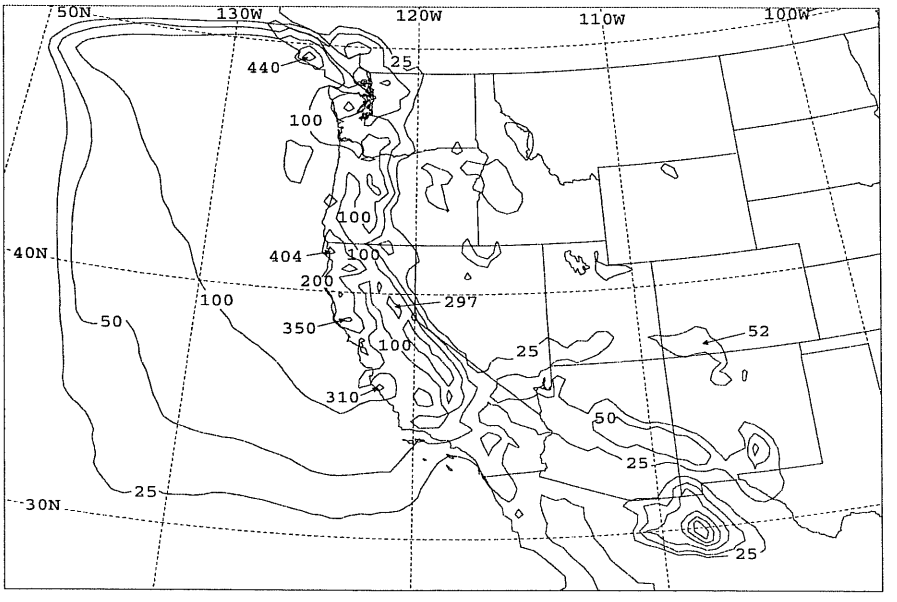

FIG. 6. Simulated precipitation (mm month^{-1}) for the DJF period in the hindcast.

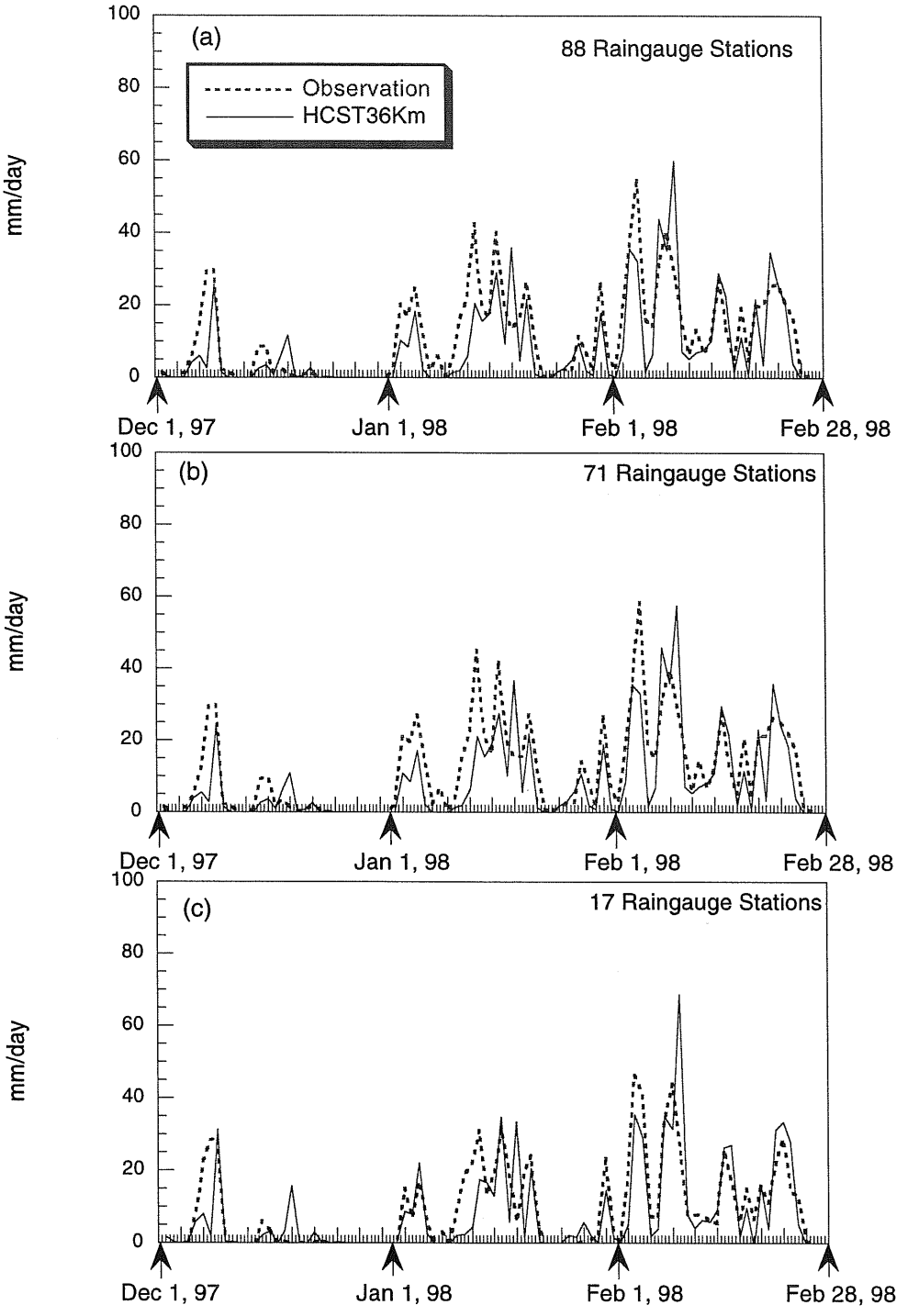

FIG. 7. Daily mean precipitation (mm day^{-1}) within California for the DJF period from the CDEC daily stations (dashed lines) and from the hindcast at a 36-km resolution: (a) all of California, (b) below 1.5-km level, and (c) above 1.5-km level.

described in the previous section. Figure 7a compares the simulated and observed daily precipitation averaged over 88 CDEC daily rain gauge stations. Precipitation during the early part of January 1998 was underestimated by as much as 50%, but the simulated timing and amount of precipitation from late January to the end of February 1998 agree well with observations. In mountainous regions, precipitation often varies as a function of elevation (Hutchinson 1970; Rhea 1976; Park and Singh 1996; Isakson 1996; Leung et al. 1996; Kim

1997). Such an elevation dependence of precipitation is especially important in the western United States, where a considerable portion of high-elevation precipitation is snow. Figures 7b and 7c present the observed and simulated daily precipitation averaged for the stations below and above the 1.5-km level, respectively. In both observation and simulation, in general, precipitation in low elevations exceeds precipitation in high elevations. This elevation-dependent precipitation during the 1997/98 winter is somewhat in contrast with earlier observational and numerical studies, where precipitation intensity tends to increase with elevation (e.g., Leung and Ghan 1995; Kim 1997). We suspect that such a variation in precipitation characteristics may be related to the large-scale environment. For example, Kim (1997) suggested that elevation dependence of precipitation may be more pronounced during cold storms, for which the freezing level is located below the 1-km level. Because elevation-dependent winter precipitation has an important effect on water resources in the western United States, especially in the snow budget, the relationship between the large-scale storm environment and the local precipitation characteristics needs further study.

We examined the simulated precipitation in six subregions in California using basin-specific monthly rain gauge data (Table 2). The six subregions were selected to account for north–south and east–west variations of precipitation along the major orographic features within California. The basin-specific monthly precipitation data and other hydroclimate data sets for California were available at the time of writing online at http://cdec.water.ca.gov. The hindcast simulated well the geographical variation of precipitation in California, at least qualitatively, during the DJF period. Figure 8 compares the observed and simulated monthly precipitation in each subregion in Table 2. The hindcast simulated well the observed monthly variation of precipitation in the six subregions, for which December was the driest and February was the wettest. Precipitation was systematically underestimated in the central and southern California coast throughout the season, most seriously in the southern California Coast Ranges, for which the simulated precipitation amount was less than 50% of the observation for all three months. This result again indicates that orography along the central and southern California coast needs much finer resolution to resolve its effects on local precipitation, as discussed earlier in this section.

The hindcast simulation has simulated well the monthly precipitation in California computed as an average of the monthly precipitation in the six regions above (Fig. 9a). The largest error occurred in January 1998, when average precipitation over the six regions was underestimated by 20%. Agreement between the simulated and observed precipitation for February, the wettest of all three months, is especially good. Figure 9b compares the observed and simulated standard deviation of precipitation calculated from all 188 monthly rain gauge stations in California (Table 2). Because of a limited number of observation points, the standard deviation in each region was not calculated. The hindcast has underestimated spatial variation of precipitation for all three months. This underestimation of spatial variability may be caused by a lack of terrain resolution. Correlation coefficients between the observed and simulated precipitation range from 0.4 to 0.75, with the lowest correlation during December 1997 (Fig. 9c). These correlation values are smaller than the values obtained in earlier studies by Soong and Kim (1996) and Kim (1997) with the same model but with a finer spatial resolution of 20 km.

Precipitation from the hindcast was processed using the method described in section 2 to run a stream flow simulation for the Hopland basin. This basin has been one of our intensive research areas, and TOPMODEL has been well tested for this basin (Miller and Kim 1996; Kim et al. 1998a; Miller et al. 1999). The lower part of Fig. 10a compares the daily stream flow from observations (gray bars) and two TOPMODEL simulations: a verification simulation using observed daily precipitation (dashed line), and the coupled hindcast simulation using the MAS-simulated precipitation (solid line) at the Hopland gauge station for the DJF period. The gray bars and solid line in the upper part of Fig. 10a represent the observed and simulated basin-average daily precipitation during the same period, respectively. The coupled hindcast has simulated well the observed daily stream flow at the Hopland gauge station with a correlation coefficient of 0.7 between the observed and simulated stream flow during the DJF period. Figure 10b compares the frequency distribution of the observed and simulated stream flow in the Hopland basin. Frequency of low flow events (less than 5 mm day^{-1}) was overestimated by 10%. The coupled simulation generally performed well for stream flow volume greater than 5 mm day^{-1}. Small sample sizes for the mid-to-high flow regime did not allow for a conclusive evaluation. Using the observed basin-average precipitation as input, TOPMODEL has reproduced closely the observed stream flow. Figure 10c compares daily stream flow from the observation and verification simulations for the DJF period with a correlation coefficient of 0.88. This result indicates that the parameter set obtained for this basin is reasonably accurate. Hence, the error in the coupled hindcast is due mainly to errors in the simulated precipitation.

5. Seasonal prediction experiment

This seasonal hydroclimate prediction study for the 1997/98 winter was designed to examine the coupling of numerical models for regional-scale seasonal climate predictions and to evaluate the prototype seasonal forecast system. This multiinstitutional collaborative study was organized as in Fig. 1 (dashed arrows). The seasonal forecast starts with the tropical SST anomaly forecast

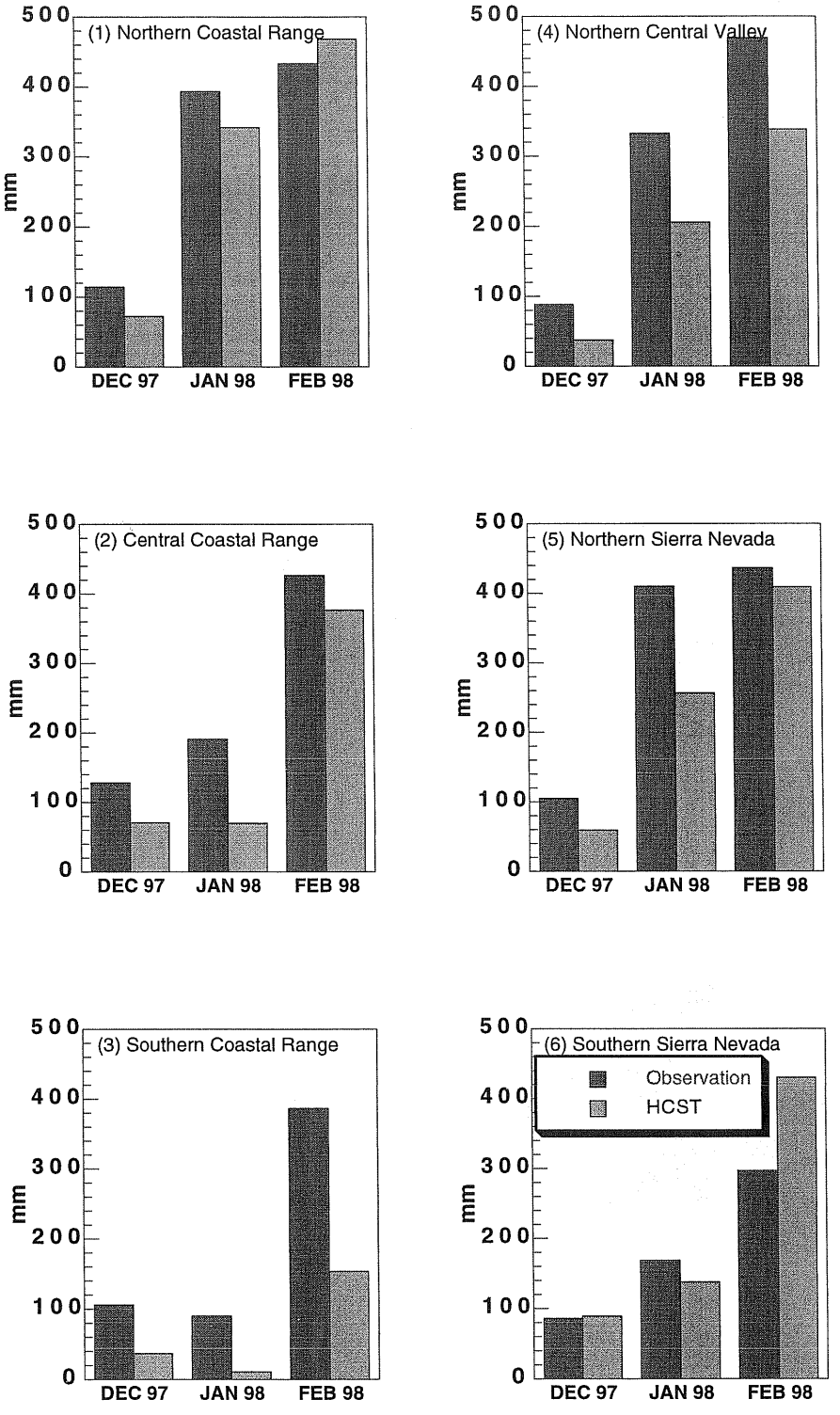

FIG. 8. Observed (black bars) and simulated (gray bars) monthly precipitation in six regions within California.

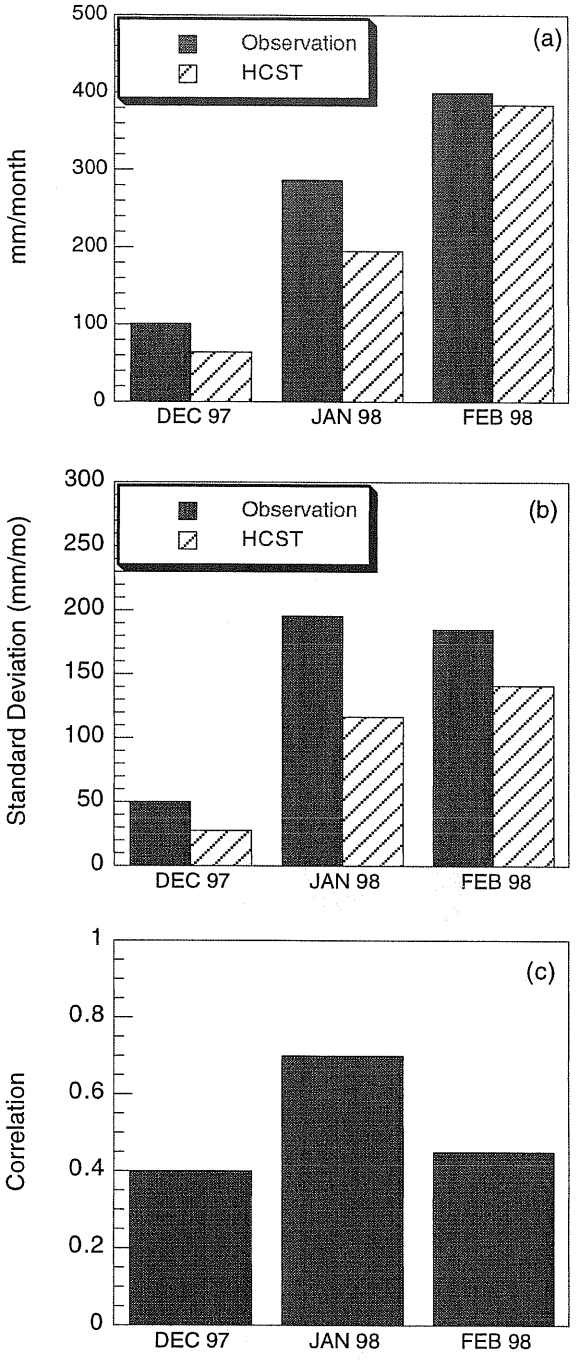

FIG. 9. Observed (black bars) and hindcast (gray bars) precipitation characteristics in California.

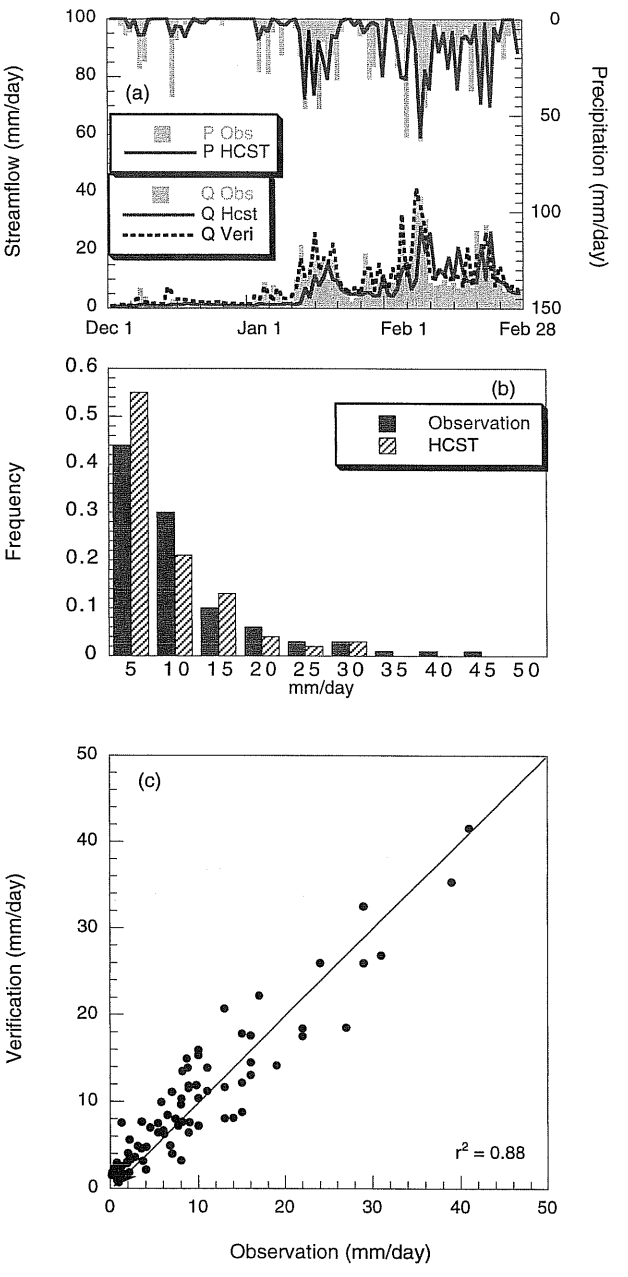

FIG. 10. (a) Observed (gray bars) and simulated (solid line) daily stream flow at the Hopland gauge station during DJF. (b) Observed (black bars) and simulated (gray) frequency distribution of the daily discharge rate at the Hopland gauge station. (c) Comparison of the daily stream flow from observations and a verification simulation in which TOPMODEL was driven with the observed daily precipitation.

by NCEP, which was made available on 15 October 1997. The predicted SST anomaly field then was used to drive the UCLA AGCM to produce a global prediction for the 1997/98 winter at a 2.5° × 2° resolution from nine ensemble simulations. As the final step, RCSM used the 12-h GCM output data from one member of the ensemble forecast for the DJF period to produce a regional forecast. Because of a lack of computational resources, we did not attempt to construct an ensemble of downscaled seasonal prediction.

a. GCM prediction

Two-tier predictions of the seasonal-scale global atmospheric circulation during winter 1997/98 were performed using the UCLA AGCM in conjunction with the

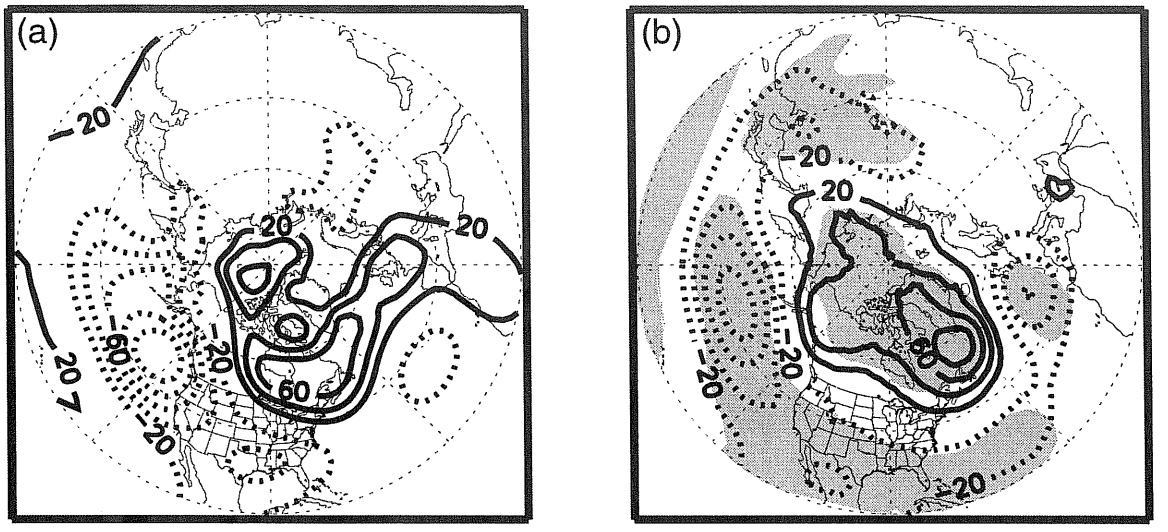

FIG. 11. (a) Observed and (b) AGCM-predicted 700-hPa geopotential height anomalies for DJF. Gray shading means significant at 99% confidence level.

SST fields from an ensemble of predictions made with the NCEP coupled atmosphere–ocean GCM (Ji et al. 1998). For this seasonal prediction, we used the 2° lat × 2.5° long, 29-layer version of the model. The global ensemble simulations have nine members, each covering a 7-month period from October 1997 to April 1998 and starting from slightly different initial conditions. A nine-member control ensemble ("control") is based on the global sea-ice and SST (GISST) climatological SST (Rayner et al. 1995). A nine-member prediction ensemble ("forecast") was generated from the same set of simulations with a modified SST field generated by adding the NCEP predicted SST anomalies to the GISST climatological values for the tropical Pacific Ocean (30°S–25°N, 120°–290°E).

The lower-tropospheric flow anomalies, as represented by the 700-hPa height anomalies defined as the difference between the forecast and control ensemble means, for the DJF period were simulated realistically. Figure 11 presents 700-hPa geopotential height anomalies from the NCEP–NCAR reanalysis and the forecast ensemble. The gray shading denotes regions where the anomalies are statistically significant at the 99% level. The largest anomaly pattern, in both the observation and prediction, is located over the Pacific–North America sector. The pattern of anomalies in this region is broadly characterized by large negative values in the midlatitude Pacific that extend eastward across the southern United States, large positive values over much of Canada, and small positive values in the subtropical Pacific. The observed pattern has the negative anomaly center of −110 m in the Pacific centered at 45°N, 140°W and the positive anomaly center of +70 m over eastern Canada. The forecast 700-hPa height anomaly pattern shows a negative anomaly center near 45°N, 165°W, 25° west of the observed position. Positive anomalies cover all of Canada and Alaska in the forecast. To quantify the overall skill of the forecast, we computed the anomaly correlation between the simulated and observed 700-hPa height anomalies for the region 20°–60°N, 180°–300°E. We obtained an anomaly correlation value of 0.71, which suggests that the forecast generally was realistic in the extratropical North Pacific–North America region.

The AGCM-predicted precipitation (mm month^{-1}) for the DJF period is presented in Fig. 12. In comparison with the observations (Figs. 6a,b) and the MAS simulation (Fig. 5), the AGCM predicted precipitation agrees well with the NCDC analysis at a 1° × 1° resolution (Fig. 6a) with somewhat smaller magnitude. One noticeable difference between the AGCM predicted precipitation and the observed precipitation is that the location of the maximum precipitation is shifted southward, in central California rather than in northern California. This southward shift is consistent with the differences between the observed and forecast 700-hPa height anomalies over western North America (Fig. 11). Nevertheless, values greater than 150 mm month^{-1} cover a large portion of northern and central California, with values greater than 100 mm month^{-1} throughout southern California. A more detailed description of these results and those of other ensembles that used the observed SSTs is given in Farrara et al. (2000).

b. Downscaled RCSM prediction

The downscaled seasonal hydroclimate prediction for the western United States was made for a single AGCM forecasted scenario because of limited computational resources. We nested the RCSM within the σ-layer grid of the UCLA AGCM fields. Nesting the RCSM within the σ-layer grid, not within the pressure-level grid as

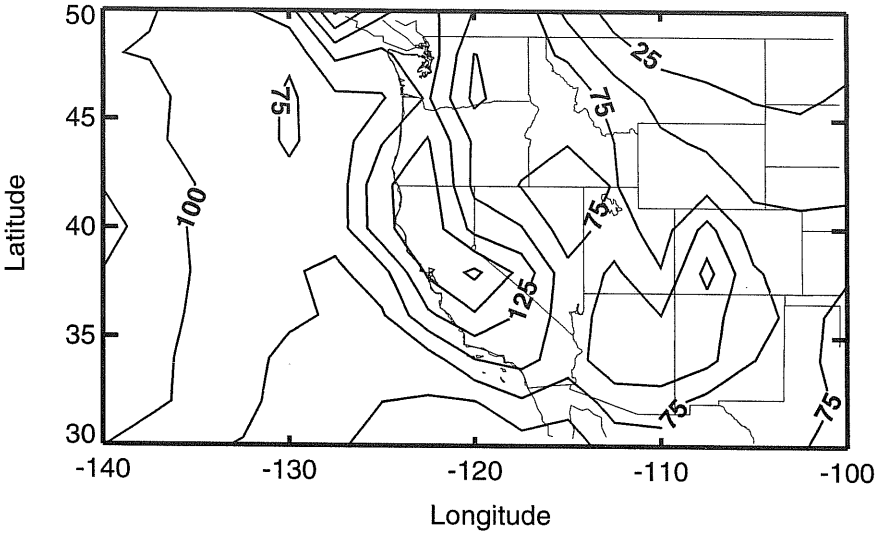

FIG. 12. AGCM-predicted precipitation [mm (30 days)$^{-1}$] over the western United States during DJF.

for the hindcast experiments, allowed us to preserve better the AGCM-produced forcing by eliminating a need for an additional interpolation from the σ levels to the pressure levels.

The downscaled seasonal prediction was successful in predicting important precipitation features in the western United States during DJF (Fig. 13). The downscaled seasonal forecast accurately predicted the locations of local precipitation maxima in the northern California Coast Ranges, the Cascades, and the Sierra Nevada, which maxima are not available from the GCM prediction (Fig. 12). In comparison with the hindcast (Fig. 5) and analyses (Figs. 6a,b), the seasonal forecast overestimated precipitation along the Cascades and underestimated precipitation along the California Coast Ranges. The bias in the north–south distribution of predicted precipitation along the Pacific coastal region was caused by a northward shift of the predicted storm track in the AGCM fields during January 1998.

Predicted season-total precipitation in California, av-

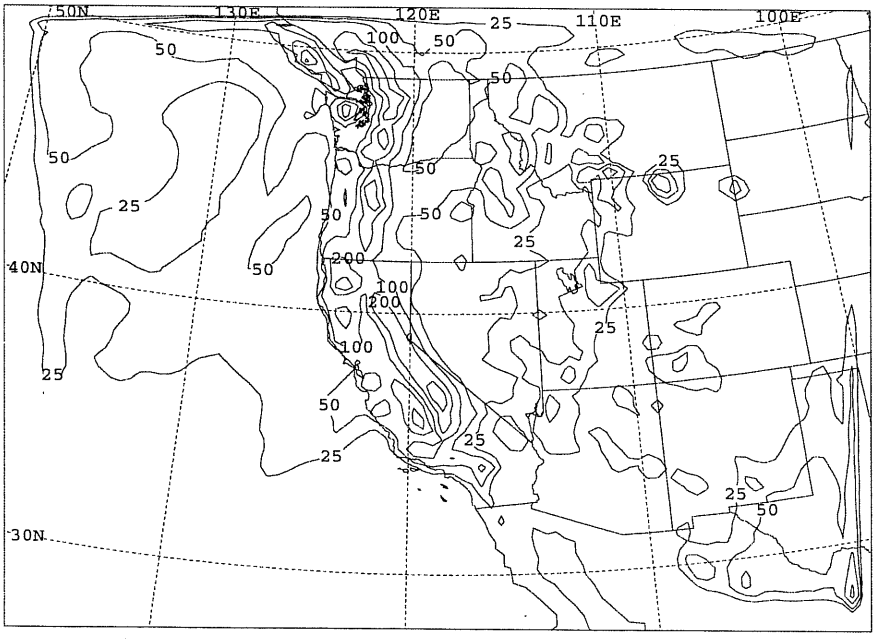

FIG. 13. Downscaled precipitation forecast [mm (30 days)$^{-1}$] over the western United States during DJF.

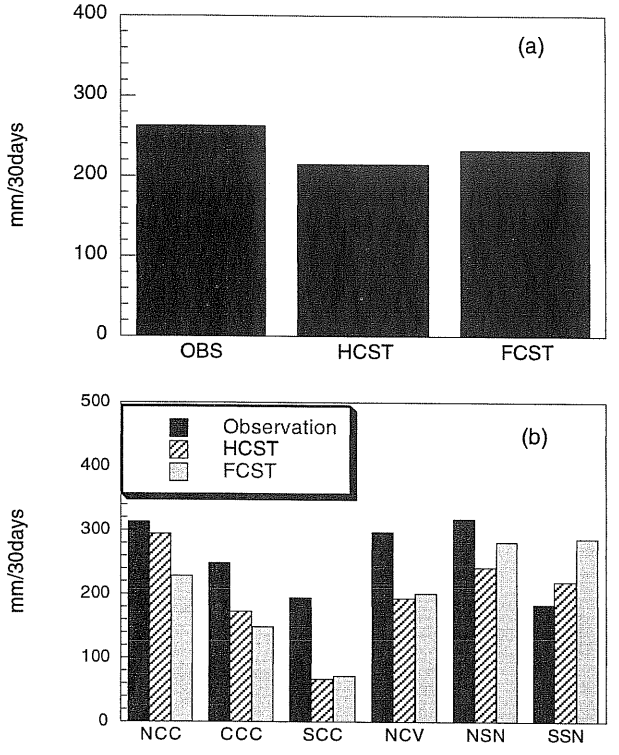

FIG. 14. (a) A comparison of the observed, hindcast, and seasonal forecast precipitation in California [mm (30 days)$^{-1}$] during DJF. (b) Observed (black bars), hindcast (striped bars), and predicted (gray bars) precipitation in six subregions within California. NCC denotes northern California coast, CCC denotes central California coast, SCC denotes southern California coast, NCV denotes northern part of Central Valley, NSN denotes northern Sierra Nevada, and SSN denotes southern Sierra Nevada.

eraged over 188 CDEC monthly stations, has underestimated slightly the observation and was comparable to the values from the hindcast simulation (Fig. 14a). The spatial distribution of the predicted DJF total precipitation also compares well with the observation and hindcast results. Figure 14b illustrates the DJF total precipitation in six California subregions (Table 2) from the observation, hindcast, and seasonal forecast. Differences between the hindcast and forecast precipitation are significant in two regions: northern California coast and southern Sierra Nevada. Forecasted season-total precipitation is similar to the hindcast results within the other four subregions (central California coast, southern California coast, northern part of Central Valley, and northern Sierra Nevada).

Figure 15 presents the DJF-total snowfall (millimeters of water per month) from the hindcast (Figs. 15a) and seasonal forecast (Fig. 15b). Because of a lack of snowfall analysis, quantitative evaluation of snowfall is not available at this time. In the hindcast (Fig. 15a), snowfall is concentrated in high-elevation areas (northern California, the Cascades, the Sierra Nevada, and central Arizona), for which snowfall maxima in northern California (Mount Shasta) and the Sierra Nevada exceed 300 mm month^{-1}. The predicted DJF-total snowfall (Fig. 15b) agrees well with the results from the hindcast simulation, at least qualitatively. Over the Sierra Nevada and the central Cascades in Oregon, predicted amounts of snowfall are close to the hindcast. Seasonal prediction greatly underestimated (overestimated) snowfall over the northern California region (northern Cascades in Washington) in comparison with the hindcast. Snowfall maxima in central Arizona also were underestimated. This difference between the hindcast and forecast snowfall was caused by northward shifts of storm tracks during January as discussed in the previous section.

Even though prediction of the DJF-total precipitation was successful, spatial and temporal variations of precipitation were not predicted well. Correlation coefficients between the observed and predicted precipitation in California were below 0.4 for all three months (Fig. 16a), much lower than the value obtained for the hindcast precipitation (0.4–0.75). The seasonal prediction overestimated precipitation in December and February, and precipitation in January was greatly underestimated (not shown). The predicted daily precipitation is comparable to observations only during the first 15 days of December and the last 15 days of February. These two periods correspond to the timescales on which predictability of a GCM is controlled by the initial conditions (early December) and by climatologically dominant modes such as the Pacific–North American pattern (late February), which is expected from the strong El Niño condition that was present during this winter, respectively (Tracton et al. 1989). This lack of accuracy in the predicted temporal and spatial variability is one of the most serious problems in applying the seasonal prediction results for other assessments such as stream flow predictions as presented below.

Figure 16b compares the frequency distribution of stream flow volume at the Hopland basin from the observations, coupled hindcast, and seasonal forecast in this study. The season-total stream flow volume from the hindcast and seasonal forecast is similar to the observation, reflecting the fact that the season total precipitation in both hindcast and seasonal forecast compares well with the observation in this basin. The predicted frequency distribution of stream flow volume, however, is considerably different from the hindcast result that generally follows the observation. The coupled seasonal stream flow prediction overestimated the occurrence of low flows (less than or equal to 5 mm day^{-1}) by a factor of 2 and underestimated the occurrence of stream flows above 5 mm day^{-1}. This shift of the predicted stream flow into the low-flow range was caused mostly by the dry January 1998 predicted by the AGCM.

6. Conclusions

The Regional Climate System Model was employed for seasonal climate hindcast and prediction for the

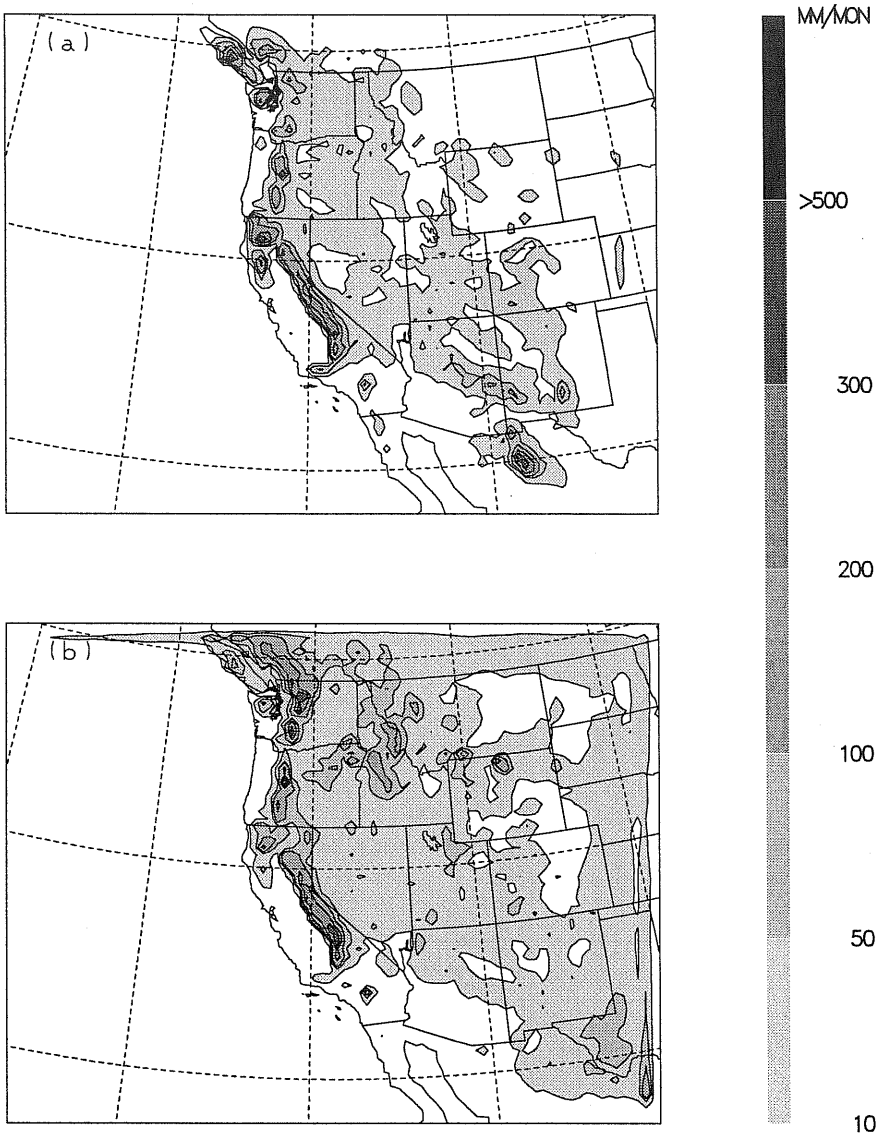

FIG. 15. Monthly mean snowfall (millimeters of water per month) from (a) the hindcast simulation and (b) the seasonal prediction experiment.

western United States during December 1997–February 1998. The main focus of this study is to evaluate the performance of RCSM for simulating hydroclimate in the western United States and to examine the performance of an experimental seasonal prediction system for the region.

In the hindcast experiment in which the RCSM was forced by the NCEP–NCAR reanalysis, good agreement was obtained between simulated and observed seasonal precipitation in the western United States. Predicted amounts and spatial distribution of precipitation in California, where rain gauge data were available for quantitative evaluations, were close to observations. Locally, precipitation on the central and southern California coast was underestimated greatly because of a lack of spatial resolution to represent narrow and steep terrain in the region. Spatial resolutions of 10 km or higher may be needed to represent properly the orographic effects on the central and southern California coast.

Using parameters from a 5-yr calibration period, TOPMODEL driven by the observed daily precipitation closely simulated the observed stream flow at the Hopland gauge station during the DJF period. The simulated stream flow from a coupled stream flow hindcast, in which daily precipitation from the seasonal hindcast was used to drive TOPMODEL, generally agreed well with observations, even though the coupled stream flow hindcast somewhat overestimated (underestimated) low

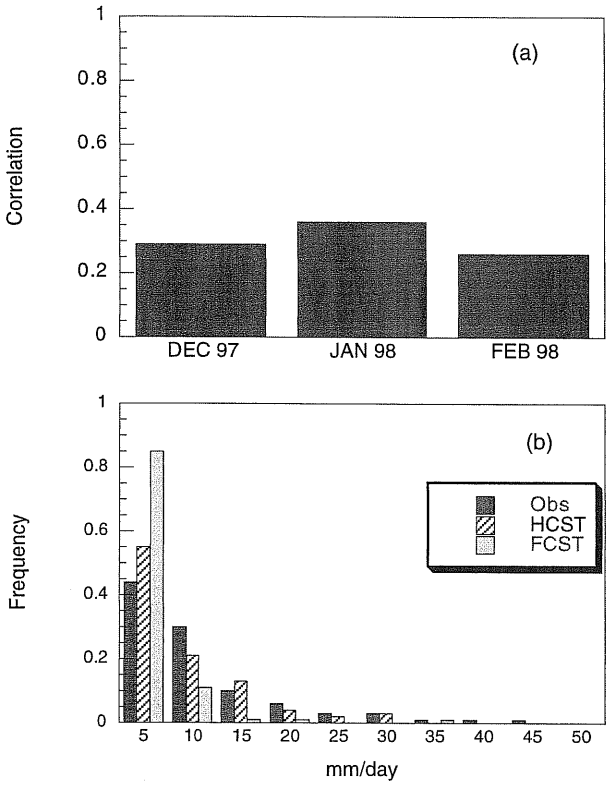

FIG. 16. (a) Monthly values of correlation coefficients between the observed and simulated (hindcast and forecast) precipitation in California. (b) Frequency distribution of stream flow from observations (dark bars), 36-km-resolution hindcast (striped bars), and seasonal prediction (gray bars).

(high) flow events. This bias in the coupled hindcast may be largely corrected by increasing the resolution of the atmospheric model.

A seasonal climate prediction experiment, in which RCSM was nested within the UCLA AGCM, produced encouraging results for predicting seasonal precipitation in the region. The qualitative features of the observed precipitation, for example, heavy precipitation along the Pacific coast, the Cascades, and the Sierra Nevada and rapid decrease of precipitation across the Cascades and the Sierra Nevada, were predicted well. For California, for which more comprehensive evaluation data are available, the predicted DJF total precipitation was comparable to the values from observations and the hindcast. The seasonal prediction, however, underestimated the spatial variability of precipitation. The predicted DJF-total snowfall agrees well with the results from the hindcast, especially over the central Cascades in Oregon and the Sierra Nevada, where heavy snowfall occurred. General overestimation of snowfall in the northern Cascades was due to northward shifts of GCM-predicted storm tracks during January 1998.

At present, our seasonal forecast experiment could produce only limited information at some level of certainty. For example, only the predictions of season-total precipitation and discharge volume were comparable to observations in this study. Temporal variation of precipitation was only useful for the first 15 days of January 1997 and the last 15 days of February 1998, perhaps because of the predictability of global models. As a consequence, short-term variations of stream flow, which are important for predicting flood potential, were not predicted correctly for the most part of the DJF period. One of the difficulties for seasonal and long-term stream flow predictions is that the variation in discharge rates depends strongly on the sequence of events that controls antecedent conditions and persistence. For the same amount of precipitation, a sequence of events with larger temporal variability has greater potential to cause flooding. Atmospheric predictability considerations strongly constrain the capability of global models to predict daily variability more than a few weeks in advance (Mass and Kuo 1998; Bengtsson 1999).

Acknowledgments. We thank California DWR and California–Nevada RFC for precipitation and stream flow data. Ms. Jung-Eun Lee helped to produce contour plots. We also thank three anonymous reviewers for useful comments. Financial support for this work was from the NASA-RESAC (NS7291), Lawrence Berkeley National Laboratory (LDRD 366139), University of California Campus Laboratory Collaboration (CLC) Project, the National Science Foundation (ATM-9630226), and the National Oceanic and Atmospheric Administration (NOAA) (GC97-286). The NCEP–NCAR reanalysis data were provided by the NOAA CIRES Climate Diagnostics Center. Computational resources were provided by the San Diego Supercomputing Center, the National Energy Research Supercomputing Center, and the NASA Office of Mission to Planet Earth, Aeronautics, and Space Sciences. Work for the U.S. Department of Energy was done under Contract DE-AC03-76SF00098.

REFERENCES

Ambroise, B., K. Beven, and J. Freer, 1996: Toward a generalization of the TOPMODEL concepts: Topographic indices of hydrologic similarity. *Water Resour. Res.*, **32,** 425–434.

Barnett, T. P., 1995: Monte Carlo climate forecasting. *J. Climate,* **8,** 1005–1022.

Bengtsson, L., 1999: From short-range barotropic modelling to extended-range global weather prediction: A 40-year perspective. *Tellus,* **51,** 13–32.

Beven, K. J., 1984: Infiltration into a class of vertically nonuniform soils. *Hydrol. Sci.,* **29,** 425–434.

——, and M. J. Kirkby, 1979: A physically based, variable contributing area model of basin hydrology. *Hydrol. Sci. Bull.,* **24,** 43–69.

——, and A. Binley, 1992: The future of distributed models: Model calibration and uncertainty prediction. *Hydrol. Proc.,* **6,** 279–298.

——, M. Kirkby, N. Schoffield, and H. Tagg, 1984: Testing a physically-based flood forecasting model (TOPMODEL) for three U.K. catchments. *J. Hydrol.,* **69,** 119–143.

Cayan, D. R., and J. O. Roads, 1984: Local relationships between

United States West Coast precipitation and monthly mean circulation patterns. *Mon. Wea. Rev.,* **112,** 163–172.

Chang, S., D. Hahn, C.-H. Yang, D. Norquist, and M. Ek, 1999: Validation study of the CAPS model land surface scheme using the 1987 Cabauw/PILPS dataset. *J. Appl. Meteor.,* **38,** 405–422.

Chen, S., J. Roads, H. Juang, and M. Kanamitsu, 1995: California precipitation simulation in the nested spectral model: 1993 January event. *Proc. Predicting Heavy Rainfall Events in California: A Symposium to Share Weather Pattern Knowledge,* Rocklin, CA, Sierra College Science Center and Floodplain Management Association, 128–133.

Duan, J., and N. Miller, 1997: A generalized power function for the subsurface transmissivity profile in TOPMODEL. *Water Resour. Res.,* **33,** 2559–2562.

Farrara, J. D., C. Mechoso, and A. Robertson, 2000: Ensembles of AGCM two-tier predictions and simulations of the circulation anomalies during winter 1997/98. *Mon. Wea. Rev.,* in press.

Giorgi, F., C. Shields Brodeur, and G. T. Bates, 1994: Regional climate change scenarios over the United States produced with a nested regional climate model. *J. Climate,* **7,** 375–399.

Green, W. H., and G. A. Ampt, 1911: Studies in soil physics. 1. The flow of air and water through soils. *J. Agric. Soc.,* **4,** 1–24.

Hong, S.-Y., and H.-L. Pan, 1998: Convective trigger function for a mass flux cumulus parameterization scheme. *Mon. Wea. Rev.,* **126,** 2599–2620.

——, and A. Leetmaa, 1999: An evaluation of the NCEP RSM for regional climate modeling. *J. Climate,* **12,** 592–609.

Hostetler, S., 1994: Hydrologic and atmospheric models: The (continuing) problem of discordant scales. *Climatic Change,* **27,** 345–350.

Hutchinson, P., 1970: A contribution to the problem of spacing raingauges in ragged terrain. *J. Hydrol.,* **107,** 643–670.

Isakson, A., 1996: Rainfall distribution over central and southern Israel induced by large-scale moisture flux. *J. Appl. Meteor.,* **35,** 1063–1075.

Ji, M., D. W. Behringer, and A. Leetmaa, 1998: An improved coupled model for ENSO prediction and implications for ocean initialization. Part II: The coupled model. *Mon. Wea. Rev.,* **126,** 1022–1034.

Kim, J., 1997: Precipitation and snow budget over the southwestern United States during the 1994–1995 winter season in a mesoscale model simulation. *Water Resour. Res.,* **33,** 2831–2839.

——, and M. Ek, 1995: A simulation of the surface energy budget and soil water content over the Hydrologic Atmospheric Pilot Experiments-Modélisation du Bilan Hydrique forest site. *J. Geophys. Res.,* **100,** 20 845–20 854.

——, and S.-T. Soong, 1996: Simulation of a precipitation event in the western United States. *Regional Impacts of Global Climate Change,* S. Ghan et al., Eds., Battelle Press, 73–84.

——, N. L. Miller, J.-H. Oh, J. Chung, and D. Rha, 1997: A regional hydrometorological prediction: Effects of cloud microphysics and terrain representation. *Proc. Second Korea–U.S. Joint Workshop on Storm- and Mesoscale Weather Analysis and Prediction,* Seoul, Korea, Atmos. Env. Research Inst., Seoul National University, 83–87.

——, ——, A. K. Guetter, and K. P. Georgakakos, 1998a: River flow response to precipitation and snow budget in California during the 1994/95 winter. *J. Climate,* **11,** 2376–2386.

——, ——, J.-H. Oh, J. Chung, and D. Rha, 1998b: Eastern Asian hydrometeorology simulation using the Regional Climate System Model. *Global Planet. Change,* **19,** 225–240.

Kim, Y., J. D. Farrara, and C. Mechoso, 1998: Sensitivity of AGCM simulations to modifications in the ozone distribution and refinements in selected physical parameterizations. *J. Meteor. Soc. Japan,* **76,** 1–55.

Lettenmaier, D. P., and T. Y. Gan, 1990: Hydrologic sensitivities of the Sacramento–San Joaquin basin, California, to global warming. *Water Resour. Res.,* **26,** 69–86.

Leung, L. R., and S. J. Ghan, 1995: A subgrid parameterization of orographic precipitation. *Theor. Appl. Climatol.,* **52,** 95–118.

——, M. S. Wigmosta, S. J. Ghan, D. J. Epstein, and L. W. Vail, 1996: Application of a subgrid orographic precipitation/surface hydrology scheme to a mountain watershed. *J. Geophys. Res.,* **101,** 12 803–12 817.

Mahrt, L., and H. Pan, 1984: A two-layer model of soil hydrology. *Bound.-Layer Meteor.,* **52,** 93–134.

Mass, C. F., and Y.-H. Kuo, 1998: Regional real-time numerical weather prediction: Current status and future potential. *Bull. Amer. Meteor. Soc.,* **79,** 253–263.

Mearns, L. O., C. Rosenzweig, and R. Goldberg, 1992: Effect of changes in interannual climatic variability on CERE-Wheat yields: Sensitivity and 2 × CO_2 general circulation model studies. *Agric. For. Meteor.,* **62,** 159–189.

Mechoso, C. R., A. Kitoh, S. Moorthi, and A. Arakawa, 1987: Numerical simulations of the atmospheric response to a sea surface temperature anomaly over the equatorial eastern Pacific Ocean. *Mon. Wea. Rev.,* **115,** 2936–2956.

——, J. Yu, and A. Arakawa, 2000: A coupled GCM pilgrimage: From climate catastrophe to ENSO simulations. General circulation model development: Past, present and future. *Proceedings of Symposium in Honor of Professor Akio Arakawa,* D. Randall, Ed., Academic Press, in press.

Miller, N. L., 1993: A hierarchical framework for coupling surface fluxes to atmospheric general circulation models: The homogeneity test. Preprints, *Conf. on Hydroclimatology,* Anaheim, CA, Amer. Meteor. Soc., 36–39.

——, and J. Kim, 1996: Numerical prediction of precipitation and river flow over the Russian River watershed during the January 1995 California storms. *Bull. Amer. Meteor. Soc.,* **77,** 101–105.

——, and ——, 1997: The Regional Climate System Model. *Mission Earth: Modeling and Simulation for a Sustainable Global System,* M. Clymer and C. Mechoso, Eds., Society for Computer Simulation International, 55–60.

——, ——, and J. Duan, 1997: The UC-LLNL Regional Climate System Model: Southwestern United States and eastern Asia studies. *Research Activities in Atmospheric and Ocean Modeling,* A. Staniforth, Ed., WMO-TD-No. 792, World Meteor. Org., 7.41–7.42.

——, ——, R. K. Hartman, and J. D. Farrara, 1999: Downscaled climate and streamflow study of the southwestern United States. *J. Amer. Water Res. Assoc.,* **35,** 1525–1537.

Nash, J. E., and J. V. Sutcliffe, 1970: River flow forecasting through conceptual models. I: A discussion of principles. *J. Hydrol.,* **10,** 282–290.

Pan, H., and L. Mahrt, 1987: Interaction between soil hydrology and boundary layer development. *Bound.-Layer Meteor.,* **38,** 185–202.

——, and W. Wu, 1995: Implementing a mass flux convection parameterization package for the NCEP medium-range forecast model. NMC Office Note, 40 pp. [Available from NCEP/EMC, 5200 Auth Road, Camp Springs, MD 20764.]

Park, J., and V. Singh, 1996: Temporal and spatial characteristics of rainfall in the Nam River dam basin of Korea. *Hydrol. Proc.,* **10,** 1155–1171.

Rayner, N., C. Folland, D. Parker, and E. Horton, 1995: A new global sea-ice and sea surface temperature (GISST) dataset for 1903–1994 for forcing climate models. Internal Note 69, November, Hadley Centre, U.K. Met. Office, 14 pp. [Available from The Met. Office, London Road, Bracknell, Berkshire RG12 2SY, United Kingdom.]

Rhea, J., 1976: Orographic precipitation model for hydrometeorological use. Ph.D. thesis, Colorado State University, 198 pp.

Roads, J. O., S.-C. Chen, A. K. Guetter, and K. P. Georgakakos, 1994: Large-scale aspects of the United States hydrologic cycle. *Bull. Amer. Meteor. Soc.,* **75,** 1589–1610.

Seibert, J., K. Bishop, and L. Nyberg, 1997: A test of TOPMODEL's ability to predict spatially distributed groundwater levels. *Hydrol. Proc.,* **11,** 1131–1144.

Sivapalan, M., E. F. Wood, and K. J. Beven, 1990: On hydrologic similarity, 3. A dimensionless flood frequency model using a

generalized geomorphologic unit hydrograph and partial area runoff. *Water Resour. Res.,* **23,** 2266–2278.

Soong, S.-T., and J. Kim, 1996: Simulation of a heavy precipitation event in California. *Climatic Change,* **32,** 55–77.

Suarez, M. J., A. Arakawa, and D. A. Randall, 1983: The parameterization of the planetary boundary layer in the UCLA general circulation model: Formulation and results. *Mon. Wea. Rev.,* **111,** 2224–2243.

Takacs, L., 1985: A two-step scheme for the advection equation with minimized dissipation and dispersion errors. *Mon. Wea. Rev.,* **113,** 1050–1065.

Tracton, M. S., K. Mo, W. Chen, E. Kalnay, R. Kistler, and G. White, 1989: Dynamical extended range forecasting (DERF) at the National Meteorological Center. *Mon. Wea. Rev.,* **117,** 1604–1635.

Wilby, R. L., T. M. L. Wigley, D. Conway, P. D. Jones, B. C. Hewistson, J. Main, and D. S. Wilks, 1998: Statistical downscaling of general circulation model output: A comparison of methods. *Water Resour. Res.,* **34,** 2995–3008.

Wood, E. F., M. Sivapalan, and K. Beven, 1990: Similarity and scale in catchment storm response. *J. Hydrol.,* **102,** 29–47.